SHEP-12-37

Uncovering quasi-degenerate Kaluza-Klein Electro-Weak gauge bosons with top asymmetries at the LHC

Elena Accomando, Ken Mimasu and Stefano Moretti

School of Physics & Astronomy, University of Southampton, Highfield, Southampton SO17 1BJ, UK

arXiv:1304.4494v1 [hep-ph] 16 Apr 2013

ABSTRACT

By exploiting the correlation between charge and spin polarisation asymmetries in $t\bar{t}$, we show that combining the two observables could identify the presence of quasi-degenerate states in a resonant signal at the LHC. As an example, we investigate experimental signatures emerging in top-antitop final states in the context of a model where the Standard Model Electro-Weak sector is allowed to propagate in large extra–dimensions of TeV^{-1} size while the colour sector is localised. Assuming current experimantal constraints from the 7 and 8 TeV runs and taking into account the estimated top (anti-top) reconstruction efficiencies, we find that the 14 TeV upgraded LHC with the planned integrated luminosity L =100 fb^{-1} could access these quasi-degenerate multiple resonances and explore for the first time the rich phenomenology in the asymmetry observables. The main outcome would be having measurable quantities, complementary to the usual total and differential cross sections, capable of distiguishing a quasi-degenerate multiply resonant spectrum from a 'standard' single resonance that could present a similar signal in a bump hunt analysis.

April 17, 2013

1 Introduction

Extra gauge bosons are among the most common ingredients of Beyond the Standard Model (BSM) scenarios motivated by a variety of extensions of gauge and/or space-time symmetries. Furthermore, resonant physics is one of the primary and straightforward sectors in which searches for such new physics are undertaken at modern collider experiments. It is also already well known that, aside from traditional differential cross section observables, more involved quantities like asymmetries can provide additional probes with which to analyse the properties of such objects, should they be observed at the Large Hadron Collider (LHC). In this paper we discuss a study of multiple neutral gauge bosons in regimes where the traditional 'bump-hunt' searches are not sufficient to observe the presence of all of the resonant states due to a mass quasi-degeneracy more severe than the mass resolution of the search channel. Using a model of extra dimensions as an example, we find that – once again – asymmetries come to the fore and can allow for the distinction between the presence of one and multiple (two in our case) resonant states.

The existence of large extra dimensions compactified in the TeV range [1], for which the fundamental string or quantum gravity scale is in turn rather low [2]–[6], is a scenario easily testable at the LHC. Further, if one dismisses the traditional assumption that all Standard Model (SM) gauge bosons propagate in the same compact space [7]–[12] and instead allow for the more general case whereby the SM gauge structure arises from branes extended in different compact directions, one realises a scenario that provides an ideal testbed for our purposes. Specifically, a general setup in which (quasi-)degenerate resonances are likely to occur is in such models of extra dimensions with relatively large compactification scales, R^{-1}. Allowing the gauge sector to propagate in the bulk typically results in strong limits on the compactification scale coming from lower mass bounds on Kaluza-Klein (KK) excitations from resonance searches or Electro-Weak Precision Tests (EWPTs) depending on the specific localisation of different parts of the fermion sector. Since the tree-level KK masses of the gauge bosons are multiples[1] of R^{-1}, one may expect that the KK EW gauge sector of such a theory would be near-degenerate since $R^{-1} >> g(g')v$ where $g(g')$ and v denote the $SU(2)_L(U(1)_Y)$ gauge couplings and the Higgs vacuum expectation value of the SM respec-

[1]This is true for the case of one extra dimension of compactification radius R, but depends on the specific compactification volume in the case of more than one extra dimension, although the compactification scales still remain the only parameters that define the approximate scale of the KK masses. We assume here the case of one flat extra dimension for simplicity.

tively. Later on, we will discuss the fact that particles that propagate in the bulk in such models generically incur loop-induced mass splittings that can be important, particularly at high compactification scales.

Within this construct, we find a realisation which complies with current stringent bounds from dijet and $t\bar{t}$ events emerging after the 7 and 8 TeV runs yet remains accessible at the 14 TeV stage. This is the one where only the EW gauge bosons can appear as KK excitations, but not the gluons. In addition, one can localise matter fermions in such a way that the production of leptonic final states is depleted with respect to that of both light and heavy quarks, as the latter are notoriously less accessible than the former in the LHC environment. In these conditions then, which can be realised in a Type I picture of the brane-world scenario, given that the sensitivity of LHC data is maximal to either processes induced by Quantum Chromo-Dynamics (QCD) effects (as opposed to those due to EW interactions) or to very clean final states involving only leptons (as opposed to both light and heavy quarks), one is not confronted with the very stringent bounds that would emerge if gluons (necessarily yielding dijet and $t\bar{t}$ final states) propagated in the large extra dimensions or EW gauge bosons propagating therein could decay in leptons. Therefore, the investigation of the effects of the extra-dimensional propagation of the EW gauge bosons yielding both light and heavy quarks in the final state remains viable also in the light of the most recent data.

It is the purpose of this paper to investigate the case of the neutral EW gauge bosons, i.e., the $U(1)_Y$ and $SU(2)_L$ states of the SM, γ and Z, and their KK excitations (or admixtures thereof), henceforth denoted as $\tilde{\gamma}'$ and $\tilde{Z}'$, respectively, produced from quark-antiquark scattering at the LHC and yielding top-antitop pairs in the final state. After accounting for existing lower bounds on the compactification scale from direct searches in di- and $t\bar{t}$ data samples generated at 7 and 8 TeV, we show that one will be able to observe at least the first excitation of the EW states at the 14 TeV stage in $t\bar{t}$ final states. Further, while the extraction of information on the additional excitations would be desirable to disentangle the extra-dimensional model from alternative new physics scenarios, we prove that the ability of defining both charge and spin asymmetries in $t\bar{t}$ final states (unlike the case of dijets) can potentially disentangle the two states (despite these appearing degenerate and unresolvable in the invariant mass distribution), consequently distinguishing this BSM scenario from ones involving individual resonances (like, e.g., Z' models). Finally, we will also illustrate that such a method can be adapted to other models showing a similar spectrum configuration,

by borrowing similar results from previous literature of ours [13].

The plan of the paper is as follows. In the next section we define the observables and discuss their dependence on the couplings of neutral resonances, which we exploit to differentiate these from single resonance models. Sect. 3 describes the model that we use as an example in more detail, establishing a scenario that lies outside of current LHC limits. In Sect. 4 we present our findings and we conclude in Sect. 5.

2 Asymmetries

In this section we define the two asymmetry observables exploited to distinguish a model with degenerate resonances from generic scenarios containing a single resonance. The ability of asymmetries to go beyond simpler observables like differential cross sections lies in their special dependence on the couplings of the exchanged particles, as extensively studied in our previous work for the case of s-channel vector bosons [13]. In this case, overlapping resonances – unresolvable in the positive definite cross section – can induce asymmetries of different sign. As we will show, this feature means that the presence of multiple degenerate resonances affects the observables in a way which cannot be reproduced by the physics of any single resonance. Our study incorporates statistical uncertainties on an asymmetry observable, A, generically defined in terms of the number of Forward (F) and Backward (B) events for an integrated luminosity $\mathcal{L}$, i.e., $N_F = \mathcal{L}\,\sigma_F$ and $N_B = \mathcal{L}\,\sigma_B$, as

$$\delta A \equiv \delta\left(\frac{N_F - N_B}{N_F + N_B}\right) = \sqrt{\frac{4}{\mathcal{L}\varepsilon}\left(\frac{\sigma_F \sigma_B}{\sigma^3_{\text{Total}}}\right)}. \tag{1}$$

We also define an illustrative measure of statistical 'significance' of an asymmetry prediction for the signal A_S as the number of standard deviations it lies away from the background prediction, A_B,

$$s = \frac{|A_S - A_B|}{\sqrt{\delta A_S^2 + \delta A_B^2}}. \tag{2}$$

within the confines of our parton-level analysis.

2.1 Charge Asymmetry

Charge or spatial asymmetry in collider physics is a measure of the symmetry of a particular process under charge conjugation. For a neutral current interaction, Charge-Parity (CP)

invariance translates this into an asymmetry in the angular dependence of the matrix element for the production of a two body final state. The Tevatron, being a $p\bar{p}$ collider, is an ideal place to measure spatial asymmetries since the polar angle in the collider frame can more or less be identified with that of the Centre-of-Mass (CM) frame, modulo Parton Distribution Function (PDF) effects. Statistically, both incoming partons will be valence quarks and an absolute preferred direction can be unambiguously defined. The definition of a charge asymmetry at the LHC becomes somewhat more involved since the pp initial state is C-invariant, necessitating the redefinition of the measured quantity itself. In this case, no preferred direction can be defined because the incoming quark will generally be a valence quark, while the antiquark must come from the sea. However, one can exploit the fact that the incoming quark will statistically carry a larger momentum fraction than the antiquark, resulting in a correlation between the boost of the $t\bar{t}$ system and the direction of the incoming quark. This property can be exploited in a number of ways, our choice here being to define the asymmetry with respect to the angle θ^*: the angle in the CM frame between the outgoing lepton and the z-axis defined, on an event by event basis, to be the direction in which the $t\bar{t}$ system is boosted [14]. This quantity, which we call A^*_{FB}, is thus defined as follows:

$$A^*_{FB} = \frac{N_{t(\bar{t})}(\cos\theta^* > 0) - N_{t(\bar{t})}(\cos\theta^* < 0)}{N_{\text{Total}}}, \tag{3}$$

where $N_{t(\bar{t})}$ denotes the number of tops(antitops) observed in the forward ($\cos\theta^* > 0$) or backward ($\cos\theta^* < 0$) direction and N_{Total} is the total number of events. In QCD, the asymmetry for the $t\bar{t}$ final state is generated dominantly at Next-to-Leading Order (NLO) via interference of leading order $q\bar{q} \to t\bar{t}$ with the corresponding box diagram as well as by the interference between initial and final state gluon radiation [15]. There are also genuine tree-level EW contributions as well as mixed EW and QCD effects at NLO [16].

2.2 Spin Polarisation

One of the benefits of the $t\bar{t}$ final state is the fact that, as particles that decay before hadronising, several observables can be defined that probe the helicity structure of one or both of the outgoing (anti)tops. The most powerful such observable is the spin polarisation, A_L, or single spin asymmetry, defined as follows:

$$A_L = \frac{N(-,-) + N(-,+) - N(+,+) - N(+,-)}{N_{\text{Total}}}, \tag{4}$$

where N denotes the number of observed events and its first(second) argument corresponds to the helicity of the final state particle(antiparticle). It singles out one final state particle, comparing the number of its positive and negative helicities, while summing over the helicities of the other antiparticle (or vice versa). The observable can be extracted as a coefficient in the angular distributions of the decay products of the parent top (anti)quark [17].

2.3 Reconstruction

While the $t\bar{t}$ channel offers a wide choice of observables that are sensitive to new physics, one of the primary complications of such analyses is the difficulty in reconstructing the 6-body final state that results from the pair production of tops. Ideally, one would perform a full chain of event generation, showering and hadronisation, culminating in a detector simulation to get an accurate representation of the reconstruction process for observables of interest. The associated efficiencies will depend on the information required for the observable and the particular decay channel of the $t\bar{t}$ system. Since our analysis is limited to be at parton level, without subsequent decay of the tops, it is necessary for us to employ reasonable estimates of reconstruction efficiencies such that our qualitative predictions correspond better to the reality of a detector environment. We estimate this quantity in a conservative manner by gauging the efficiencies of the primary requirements of each observable in each decay channel and using a net efficiency weighted by the branching fractions.

The common experimental requirement between the two asymmetry observables of interest and also the invariant mass distribution is a full reconstruction of the $t\bar{t}$ system. The only extra information needed for the asymmetries is the angular distributions of the decay products of one or two the tops when extracting the top spin observables. An important consideration for the analysis of new physics at several TeV is the likely boosted nature of the final states which will have an impact on the reconstruction process. The collimation of decay products means that many traditionally reliable measurements such as b-tagging, invariant mass reconstruction and isolation become hampered and must be adjusted. A variety of pruning and jet substructure methods are applied at the LHC [18] and quote efficiencies of about 30-40% to tag a hadronic top and a number of analyses have used such methods in recent resonance searches [19], showing that including the boosted methods increases sensitivity to higher Z' masses. The weighted efficiencies are quoted to be around 5 or 6% from each of the fully hadronic and semi-leptonic channels. As yet, we are not aware of any asymmetry measurements nor analyses in the dilepton channel using these techniques. We

therefore choose a total 10% efficiency as a conservative estimate to reconstruct high mass $t\bar{t}$ events.

The charge asymmetry measurement can be made in any of the three $t\bar{t}$ decay channels and a reconstruction of the top four momenta, after potential top-tagging using boosted methods, is sufficient to obtain the quantity and nothing extra is needed beyond sufficient statistics to represent it as a function of $M_{t\bar{t}}$. We therefore use the same reconstruction efficiency estimate for this observable as used in the resonance searches. The top polarisation asymmetry is more complicated due to the need for reconstructing the angular distributions of decay products. What is clear is that the boosted systems will inhibit the measurement of such a quantity as the collimation of the decay products approaches the angular resolution of the calorimeters. At this stage, a lack of experimental analyses makes it difficult to estimate how well such a quantity can be measured at high p_T although a number of papers discuss the problem and pose potential solutions moving away form the requirement of fully reconstructing the decay products [20]. For this study, we keep the same efficiency estimate as for the other observables, bearing in mind that this may be optimistic, particulary since we cannot assess the process of extracting the coefficient from the top decay kinematics. We feel this will not greatly affect the conclusions since the capacity to distinguish degenerate resonances relies mainly on integrated rather than differential asymmetry measurements.

2.4 Asymmetries and resonance couplings

Here, we elaborate on the specific coupling dependence of the asymmetries as discussed in [13] and the expectation for multiple resonances. The unique coupling structure of the asymmetries can be traced to the fact that they access a parity asymmetric combination of left and right-handed $\tilde{\gamma}', \tilde{Z}'$ couplings, $C_R^2 - C_L^2$, as opposed to a cross section σ, which depends only on the symmetric combination, $C_R^2 + C_L^2$. For a given initial state with chiral couplings $q^i_{R,L}$ to the $\tilde{\gamma}', \tilde{Z}'$, the dependence of the observables is summarised for the $t\bar{t}$ final state as:

$$\begin{aligned} \sigma &\propto \left((q^i_R)^2 + (q^i_L)^2\right)\left(t_R^2 + t_L^2\right), \\ A_{FB} &\propto \left((q^i_R)^2 - (q^i_L)^2\right)\left(t_R^2 - t_L^2\right), \\ A_L &\propto \left((q^i_R)^2 + (q^i_L)^2\right)\left(t_R^2 - t_L^2\right). \end{aligned} \tag{5}$$

Naturally, the fact that the cross section is positive definite while the two asymmetries are not (as intimated already), being additionally sensitive to the relative 'handedness' of

the couplings, suggests that multiple resonances will be able to produce unique effects that cannot be reproduced by any single resonance. Furthermore, interference effects of the form

$$\propto \left(q_R^{(1)} q_R^{(2)} \pm q_L^{(1)} q_L^{(2)}\right) \left(t_R^{(1)} t_R^{(2)} \pm t_L^{(1)} t_L^{(2)}\right), \tag{6}$$

depending on the observable, can have a non-trivial structure, as induced by the specific couplings of the virtual objects. In essence, the effects of having two particles with different couplings and hence different widths can induce interesting lineshape effects in the asymmetry observables while still approximating a Breit-Wigner shape in the differential cross section.

3 The model

A large amount of theoretical and phenomenological literature exists on models which place the whole SM particle content [21] or sometimes only its gauge sector [8, 9] in the bulk. The main difference between the two being the delocalisation of fermions which requires an orbifold compactification in order to obtain chiral states. These can be seen as extensions of the Arkani-Hamed–Dimopoulos–Dvali (ADD) scenario, which reformulates the hierarchy problem by allowing gravity to live in the bulk while localising the rest of the SM on a brane. The framework for a model where a selection of the SM gauge structure is allowed to propagate in the bulk is motivated in [22] and represents a mixture of the two pictures. Given the choice of localising any combination of the gauge groups and matter representations, a number of combinations are possible. Our study lends itself to the (t, l, l) realisation of [22] (henceforth AADD), where t, l denote 'transverse' and 'longitudinal' and refer to the orientation of the ($SU(3)_C$, $SU(2)_L$, $U(1)_Y$) gauge groups with respect to the extra dimension. This implies that the colour sector is localised while the EW one propagates in the bulk, gaining KK excitations. In order to realise a model with scales accessible at the LHC, the leptonic sector is also allowed to propagate in the bulk. The orbifold compactification necessary to accommodate fermions in the bulk preserves KK-parity, suppressing the interactions of the EW KK resonances with the leptonic sector. This simultaneously removes the traditional di-lepton channel from searches for such resonances and limits the constraints from EWPTs that typically arise from a fully localised fermion sector. In addition, having kept the quark sector localised along with the gluons leads to an enhancement of the couplings of the KK resonances to quarks relative to its SM zero-modes as a result of the KK expan-

sion procedure. Ultimately, we are left with a model in which EW gauge bosons have KK excitations, $\tilde{\gamma}'$ and $\tilde{Z}'$, which couple universally to the quark sector with an enhancement of $\sqrt{2}$ to their SM gauge quantum numbers and have loop-suppressed interactions with the lepton sector which we neglect. As far as their interactions with quarks are concerned, these particles are heavy copies of their SM counterparts. We assume that EW Symmetry Breaking (EWSB) takes place in the bulk but that these contributions are small compared to the compactification radius as discussed in the introduction and we elaborate on the assumption of quasi-degeneracy in the next section. We therefore compute the tree-level widths of the resonances assuming only contributions from quarks with a small ($\sim 3\%$) k-factor to account for NLO QCD contributions.

We wish to use this specific realisation of an extra-dimensional model, compatible with current LHC limits, as an example of the scenario in which asymmetries can be used to deduce the presence of quasi-degenerate resonances beyond the mass resolution of the search channel. In this case, although the dijet channel represents a more sensitive mode with respect to the signal as shown in Sect. 3.2, we would like to consider $t\bar{t}$ due to the fact that one can measure both its charge and polarisation asymmetries, which turns out to be essential in identifying the presence of more than one particle. In any case, one would not expect the mass resolutions of both channels to differ greatly at such high p_T and, further, the large uncertainties associated with jet energy scale are likely to further compromise the ability to resolve nearby peaks in both invariant mass spectra.

3.1 Radiative mass corrections and mixing

A typical feature of 'universal' type models of extra dimensions, where some of the SM matter content is allowed to exists in the bulk, is that KK excitations receive radiative mass corrections beyond those that occur in a 4-Dimensional (4D) realisation. Considering one extra dimension for simplicity, these corrections originate from the violation of 5-Dimensional (5D) spacetime symmetries caused by the compactification of the extra direction [23]. 5D loop contributions which do not break these symmetries will simply contribute to the field strength renormalisation of the 5D fields. Specifically, a circle compactification violates Lorentz invariance at long distances and can accommodate loop contributions with non-zero winding number around the extra-dimensional space and yield universal, finite corrections to the two point function proportional to $\frac{1}{R^2}$ and independent of KK number. Furthermore, the orbifold projection induces yet more contributions arising from the orbifold fixed points which

violate translational invariance. Therefore, loop diagrams where a particle encounters such a boundary and flips its 5D momentum will also induce logarithmic corrections proportional to the KK mass $\frac{n}{R}$. The two types of corrections are termed 'bulk' and 'orbifold' respectively and contribute only to the 5th component of the field strength renormalisation factor which, upon KK decomposition of the action, corresponds to a mass correction to the 4D KK modes.

Consequently, the assumption that the gauge boson excitations at each KK level will essentially be degenerate with a mass of $\frac{n}{R}$ is not necessarily a good one, depending on the particular realisation of the model. The indirect importance of such mass splittings lies in the subsequent modification of the mixing between the neutral gauge bosons $\tilde{\gamma}'$ and $\tilde{Z}'$ which will, in turn, affect the exact coupling structure of the mass eigenstates. While at LO one can assume that the mixing between the hypercharge and T_3 gauge bosons will proceed identically to the SM with EWSB ($\theta = \theta_W$, where θ is the mass mixing angle between the resonances in AADD and θ_W is the Weinberg angle), mass splittings will drive the mixing back towards the pure gauge states and invalidate the assumption that such resonances will couple like 'copies' of the SM γ and Z stated in [22]. That said, in our case, the gauge bosons of interest do not interact strongly, which ensures that the splitting effects will not be too large.

For the 'Universal Extra Dimensions' (UED) realisation[2] addressed in [23], the aforementioned corrections to the neutral gauge sector masses result in a mass splitting of about 6% of the compactification scale, R. The case of AADD closely resembles a universal scenario with regards to the EW sector, the only difference being that the localisation of quarks makes them couple universally to all KK modes. Thus the mass corrections to each KK level will resemble those of UED with the 5D quark contribution removed and replaced by a normal 4D SM vacuum polarisation with enhanced couplings. As shown in [23], fermions do not contribute to the gauge boson masses via orbifold corrections which are dominant over the bulk corrections for all KK-levels, particularly with increasing R^{-1} meaning that localising quarks does not have a big effect on the mass splitting. One would also expect a negative logarithmic contribution from the localised fermion interaction of each gauge boson proportional to $g'^2 \sum_q Y_q$ and $g^2 \sum_q T(f)$ respectively, where Y denote hypercharge and $T(f)$ denotes the trace of the generators $Tr[t_A t_B]$ in the fundamental represenation of $SU(2)$. We have calculated that the corrections are small compared to those arising from the bulk particle content and decrease the mass splitting by about 1%. It is fair to say that this keeps

[2] A model where the full SM particle spectrum is allowed to propagate in the bulk [21].

the model within the quasi-degenerate regime since we don't expect the mass resolutions of the $t\bar{t}$ or dijet channels to be much better than 5%. The splitting are, however, large enough to significantly affect the mixing structure of the KK EW gauge boson couplings.

Ultimately, in the context of using asymmetries to probe observed resonances in the $t\bar{t}$ spectrum, it is evident that having too large mass splittings will first and foremost reduce the problem to a study of multiple single resonances as opposed to a quasi-degenerate spectrum. We would therefore like to consider the regime where the mass splitting could be large enough to induce non SM-like mixings (and therefore couplings) while maintaining a quasi-degeneracy in the first KK level so that the $t\bar{t}$ mass resolution does not permit one to fully resolve the two resonances in the cross section. This is chiefly because we would like to highlight the efficacy of using differential asymmetry observables to distinguish such a case from a single resonance in a way that is not possible using a differential cross section analysis. In models with a large enough mass splitting, regular resonance search methods will be sufficient to recognise the presence of two new bosons while, if not, an analysis of asymmetries will do so. We choose to present a number of results for the illustrative limit of fully degenerate resonances as a 'worst case scenario' for our purposes while also including some observables for the spectrum with radiative corrections.

An important point to make is that, while mass splittings will affect the mixing of the KK resonances, in the exactly degenerate limit, the mixing angle, θ, should not be a physical observable around the resonance peak. This is clear since the mixing of two degenerate states simply amounts to a redistribution of couplings which can only yield differences in widths coming from (small) top mass effects. With this principle in mind, we found that it was extremely important to include off-diagonal widths in order to prevent artificial effects arising when varying mixing angles. When multiple resonances have common decay channels and a mass splitting comparable to their intrinsic decay widths, it may occur that imaginary parts of one-loop diagrams mixes the two states via their width [24]. In this case, the propagators must be treated as a matrix with the off diagonal components from these loops potentially altering their resonant structure. The size of these effects is maximised in the degenerate limit and we find that including these effectively removes the mixing angle as a physical parameter up to (small) interference effects with the SM and higher KK gauge bosons. In order to highlight these points, we simulate the phenomenology of the neutral KK resonances in both extreme cases: SM like couplings γ' and Z' ($\theta = \theta_W$) and maximally 'unmixed' gauge states W_3' and B' (θ =0), which turn out to show large differences in the

asymmetry observables when not including the off diagonal effects. Since the unmixed limit corresponds in a sense to the restoration of the EW gauge symmetry, one would expect the off diagonal effects to vanish in this limit. As such, the phenomenology of the unmixed case corresponds to the 'true' observable while artifacts from not including off diagonal effects will arise once the mixing angle is switched on.

3.2 LHC limits on R^{-1}

The nature of the model ensures that the new resonances couple in an enhanced manner to quarks while simultaneously having suppressed couplings to leptons. This dictates that the strongest constraints on the model will not come from EWPTs nor traditional di-lepton resonance searches but rather from dijet and possibly top-antitop searches. With this in mind we would like to estimate the current limits on the compactification scale, R^{-1}, using the most recent LHC (CMS) analyses available in the two channels, in order to use a still-viable version of this model as our test case. We use the latest dijet resonance search for $\sqrt{s}$ =8 TeV and 19.6 fb^{-1} [25] while for $t\bar{t}$ we found the most constraining analysis to be the boosted resonance search in the lepton+jets channel at $\sqrt{s}$ =7 TeV with full luminosity [26].

Such searches determine limits on the enhancement of the 'unfolded' $t\bar{t}$ production cross section in the case of the lepton+jet search and $\sigma \times BR(Z' \to j\bar{j}) \times \mathcal{A}$ (Acceptance) for the dijet search. Both use a 'bump-hunt' binned analysis fitting the background plus a single-resonance signal shape with the cross section as a free parameter. Consequently, the analysis is rather sensitive to the signal shape. The fact that any interference effects are *a priori* neglected in model independent limits means that the limits we can obtain on our model will be in the approximate case of degenerate resonances not interfering with the SM gauge bosons, in order to best match the assumed signal shape. We therefore compute the production rate in our model as a function of R^{-1} which we equate with $M_{\tilde{\gamma}'} \approx M_{\tilde{Z}'}$ and compare these predictions with the CMS data to obtain a qualitative, yet instructive, limit on the compactification scale. In addition to neglecting the interference effects, which are indeed small compared to the QCD background, we also only consider the first KK level of resonances when computing the signal cross sections. This is also to best match the model signal shape used in the experimental analyses. The effects of the higher KK resonances are strongly reduced at high scales ($\geq$2 TeV) due to low parton luminosities while at the lowest scales ($\sim$1 TeV) the first resonance is enough to exclude the model. We note that, within these simplifications, the production rates between the SM-like mixed and unmixed cases do

not differ significantly even without including the aforementioned off-diagonal width effects. For the dijet analysis, an additional kinematical cut of pseudorapidity separation between the jets $\Delta\eta_{jj}$ <1.3 is imposed along with the requirement that both jets be central ($|\eta|$ <2.5).

In Figure 1, we compare the $t\bar{t}$ and dijet production rate in AADD to the limits quoted from CMS resonance searches in the two channels. The dijet rates are unsurprisingly large since the resonance couples with a factor $\sqrt{2}$ larger than the SM case leading to a limit of order 2.5 TeV on R^{-1}. The fact that this analysis was performed on 8 TeV data compared to 7 for $t\bar{t}$ along with the higher multiplicity of light quark final states and better reconstruction efficiency suggests that the latter analysis will not be able to compete in setting such limits. The $t\bar{t}$ limits are based on particular assumed widths (1% and 10% of the mass) of the resonances. The popular 'Topcolor' [27] benchmark model that is constrained in this analysis has been left on the figures for comparison. Given that, in our scenario, the tree-level width contributions come only from quarks and give a contribution of about 5% of the mass, we compare the predictions to both cases, understanding that the true limit will lie somewhere in between. It appears that the exclusion is rather sensitive to this assumption since, in the narrow case, AADD rates are higher than the Topcolor ones while in the wide case they are lower, which may well be a direct consequence of the ∼5% widths. This channel produces a limit on R^{-1} of about 1.5-1.7 TeV, which is much lower than the dijet case at 8 TeV, as expected. We therefore choose to simulate subsequent results for a compactification scale of 3 TeV in order to present the phenomenology of the AADD model.

4 Results

We now present our numerical results for the phenomenology of the AADD model as our benchmark for a quasi-degenerate two-resonance scenario preferentially coupled to $t\bar{t}$. As suggested by Subsects. 3.1 and 3.2, a compactification scale of $R^{-1} = 3$ TeV is chosen as our reference point simply as it is still allowed by current resonance searches. The code exploited for our study is based on helicity amplitudes, defined through the HELAS subroutines [28], and built up by means of MadGraph [29]. Initial state quarks have been taken as massless whereas for the final state top (anti)quarks we have taken $m_t = 175$ GeV. The CTEQ6L1 [30] PDFs were used with factorisation/renormalisation scale set to the compactification scale, $Q = \mu = R^{-1}$. VEGAS [31] was used for the multi-dimensional numerical integrations. In each case, the BSM signal including (small) inteference with the EW zero modes (γ,Z) is

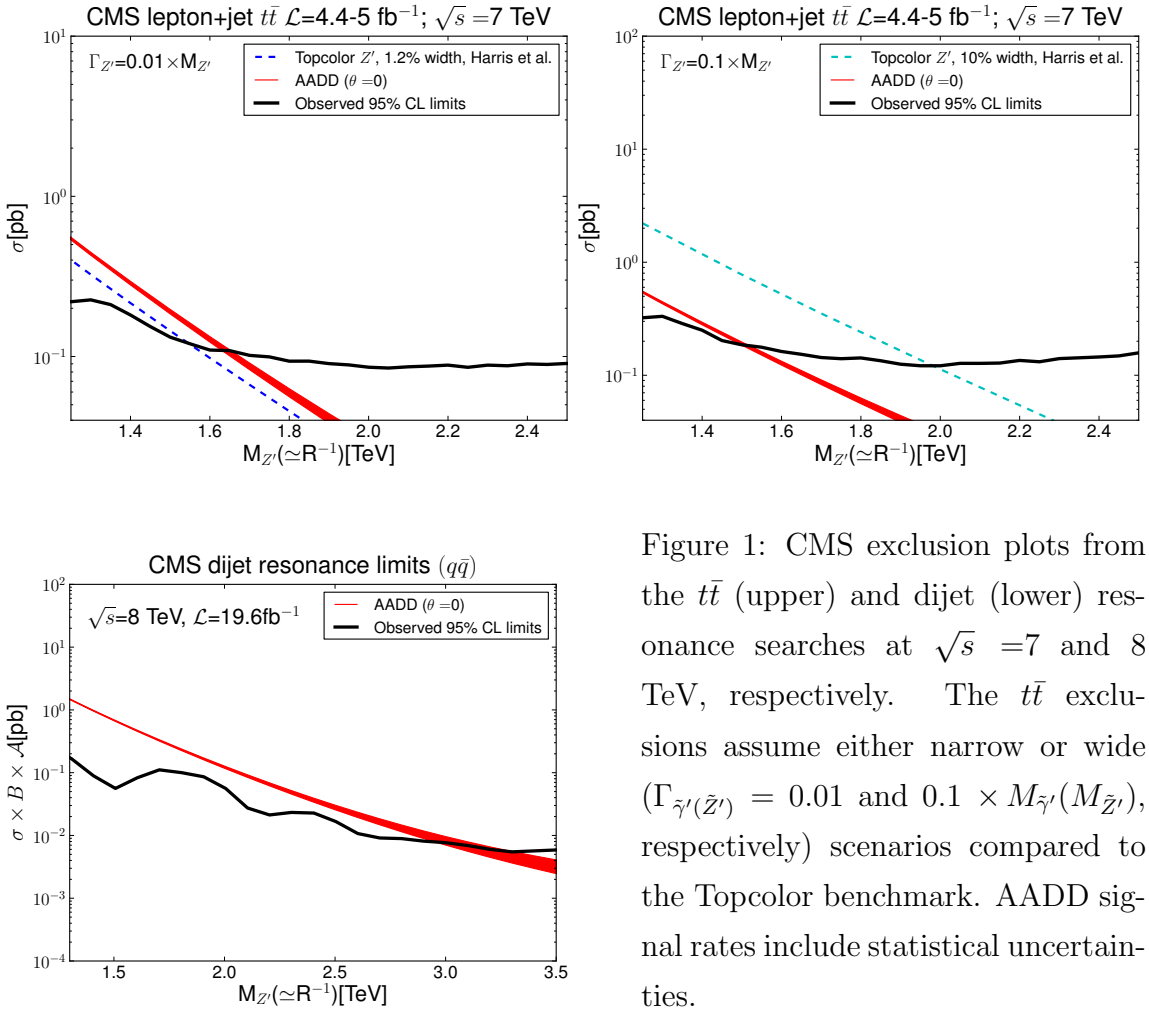

Figure 1: CMS exclusion plots from the $t\bar{t}$ (upper) and dijet (lower) resonance searches at $\sqrt{s}$ =7 and 8 TeV, respectively. The $t\bar{t}$ exclusions assume either narrow or wide ($\Gamma_{\tilde{\gamma}'(\tilde{Z}')} = 0.01$ and $0.1 \times M_{\tilde{\gamma}'}(M_{\tilde{Z}'})$, respectively) scenarios compared to the Topcolor benchmark. AADD signal rates include statistical uncertainties.

laid against the tree level SM background dominated by QCD and supplemented by EW production for completeness, all at LO. We focus on differential cross section and asymmetry observables binned around the resonance peak region in invariant mass, $|M_{t\bar{t}} - R^{-1}| < 500$ GeV. The results should not, qualitatively, be affected by the choice of R^{-1}. We will begin by showing results for the exactly degenerate limit and highlight the importance of including off-diagonal effects before moving onto the radiatively split spectrum. We will then present a comparison of the degenerate AADD model with generic single Z's in the asymmetry observables to underline the fact that they can be very useful in identifying the presence of quasi degenerate, multiple resonances when these cannot be resolved in the invariant mass spectrum.

4.1 Invariant mass and asymmetry spectra

We present invariant mass profiles in the standard cross section as well as charge and spin asymmetries for both SM-like 'mixed' ($\theta = \theta_W$) and the pure 'unmixed' ($\theta = 0$) case for the LHC at 14 TeV. The relative contributions of the two resonances to the aforementioned observables are decomposed to highlight the fact that, while the invariant mass spectrum views these as a single bump, the asymmetries may allow one to deduce the presence of multiple states. As discussed in Subsect. 3.1, the mixing parameter, θ, should not be physical in the degenerate limit. This appears to be the case for the invariant mass spectra in Figure 2, where the observable quantity in black reveals the presence of a single resonance, with both contributions and their interference adding coherently to form a Breit-Wigner-like peak. The predictions for both mixed and unmixed cases are rather similar, differing by less than 10%. The signal (S) is, unsurprisingly, very visible above the Background (B), as indicated by the large significances, $S/\sqrt{S+B}$, in the right-hand subplots even after folding in a 10% reconstruction efficiency.

In contrast, the asymmetries highlight a very different phenomenology. A clear difference can be noted between the prediction for the unmixed and mixed cases in Figures 3 and 4 respectively. This is the unphysical artifact coming from the omission of off-diagonal width contributions discussed in Sect. 3.1. Figure 5 shows that the inclusion of these effects makes the prediction for the mixed case consistent with that of the unmixed case, where the off-diagonal terms are zero by construction, restoring the mixing angle to an unphysical parameter. The predictions for the unmixed case and the mixed case with off-diagonal widths agree up to small interference effects away from the peak where the off diagonal terms become small and the latter begins to agree with the mixed case without their inclusion. These deviations are more pronounced in the asymmetries and are likely due to our approximation of only considering off diagonal effects in the denegerate first level KK resonances. We therefore analyse the unmixed scenario as representing the 'true' observables in this study.

First, we comment on the physical content of Fig. 3. In the upper-left plot, we can see that in the case of A_L, a characteristic dip appears as a consequence of the two superimposed objects having different widths and couplings. The effects from the wider resonance come in around the edges of the deviation, pushing the value of the observable towards the preferred one for its set of couplings while, near the centre of the distribution, the contribution from the narrower resonance pulls it towards the latter's preferred value. This effect is not as evident in the case of A^*_{FB}, shown in the lower left plot of Fig. 3, owing to the dominant contribution

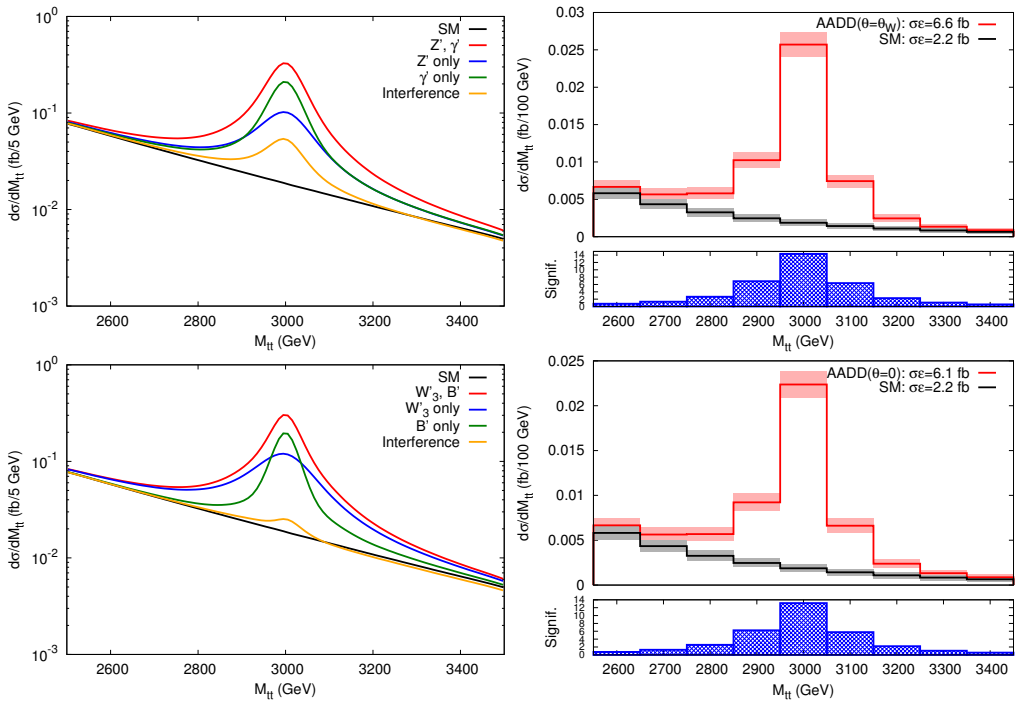

Figure 2: The $t\bar{t}$ invariant mass (M_{tt}) distribution of the cross section for the AADD model with $R^{-1} = 3$ TeV. The upper two plots show the case where the couplings are Z-like and γ-like while the lower two plots show the case where they are B-like and W_3-like. The left column highlights the contributions from the two resonances and their interference. The right column shows the observables as they would be observed at the LHC at 14 TeV, with 100 fb^{-1} of integrated luminosity, incorporating a 10% reconstruction efficiency on the $t\bar{t}$ system and statistical uncertainties. The lower subplots on the right hand side measure the bin-by-bin significance of the signal in standard deviations.

to the process coming from the up quark initial state. In the limit where only this state contributes, $A^*_{FB}(t\bar{t})$ is always positive in such a model with universal fermionic interactions, as can be inferred from Sect. 2.4. In order to give a complete description of asymmetry effects, in the two left-hand side plots of Fig. 3 the observables A_L and A^*_{FB} are decomposed into contributions from each individual resonance plotted alongside their combination compared to the SM, emphasizing the competition between them. The coupling dependence of such observables allows for this special phenomenology and these observables like to be large since the W'_3 couplings are purely left-handed, maximising the parity asymmetric coefficient in eq. (5). The right-hand side plots of Fig. 3 display the two observables, A_L and A^*_{FB},

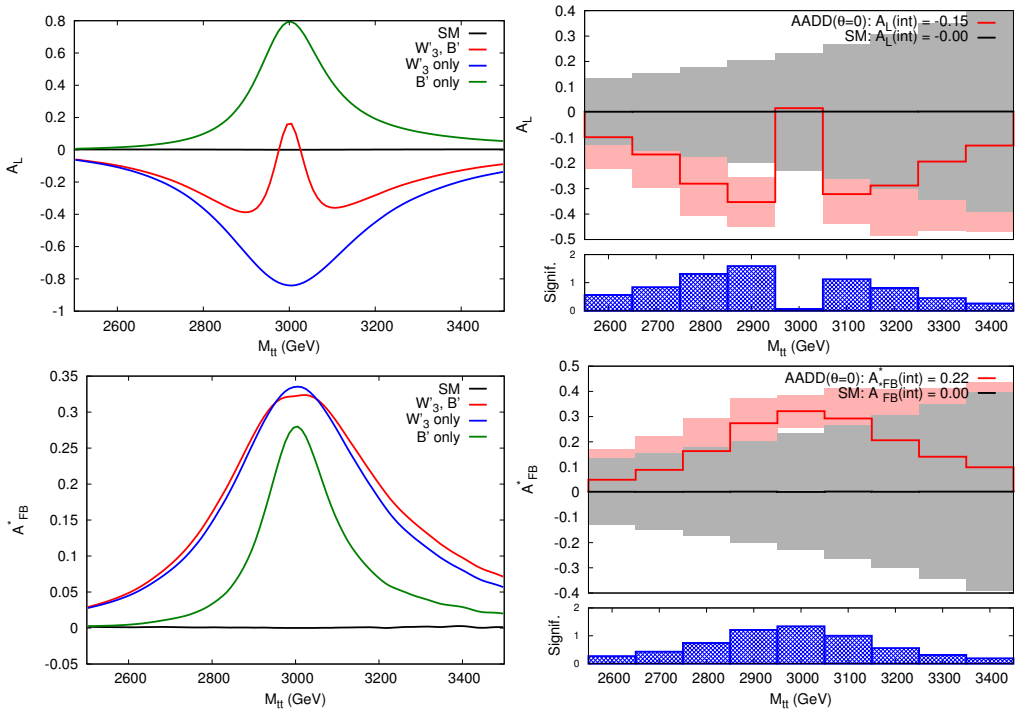

Figure 3: The $t\bar{t}$ invariant mass (M_{tt}) distribution of the A_L and A^*_{FB} asymmetries for the AADD model with $R^{-1} = 3$ TeV where the couplings are B-like and W_3-like ($\theta = 0$). The left column shows each of their contributions individually compared to the total (in red). The right column shows the observables as they could be seen at the LHC at 14 TeV, with 100 fb^{-1} of integrated luminosity, incorporating a 10% reconstruction efficiency on the $t\bar{t}$ system and statistical uncertainties. The lower subplots on the right hand side measure the bin-by-bin significance of the signal as defined in eq. (2).

with statistical uncertainties at the 14 TeV LHC after 100 fb^{-1} of integrated luminosity folding in a 10% reconstruction efficiency as mentioned in Sect. 2.3. The significances in this case are defined as in eq. (2) and are lower than those of the invariant mass distribution. Nonetheless, the signal range is rather wide and an integrated value of the observable could provide adequate statistical significance to be observable above the background prediction as we shall show later in Sect. 4.2.

Although the 'dip' feature of the AADD scenario is visible in the binned A_L figures, it is about the only thing that suggests a differing phenomenology from that of a single resonance. Furthermore, the large amount of luminosity required to achieve a more statistically significant differential analysis of asymmetry observables that could confirm the presence of

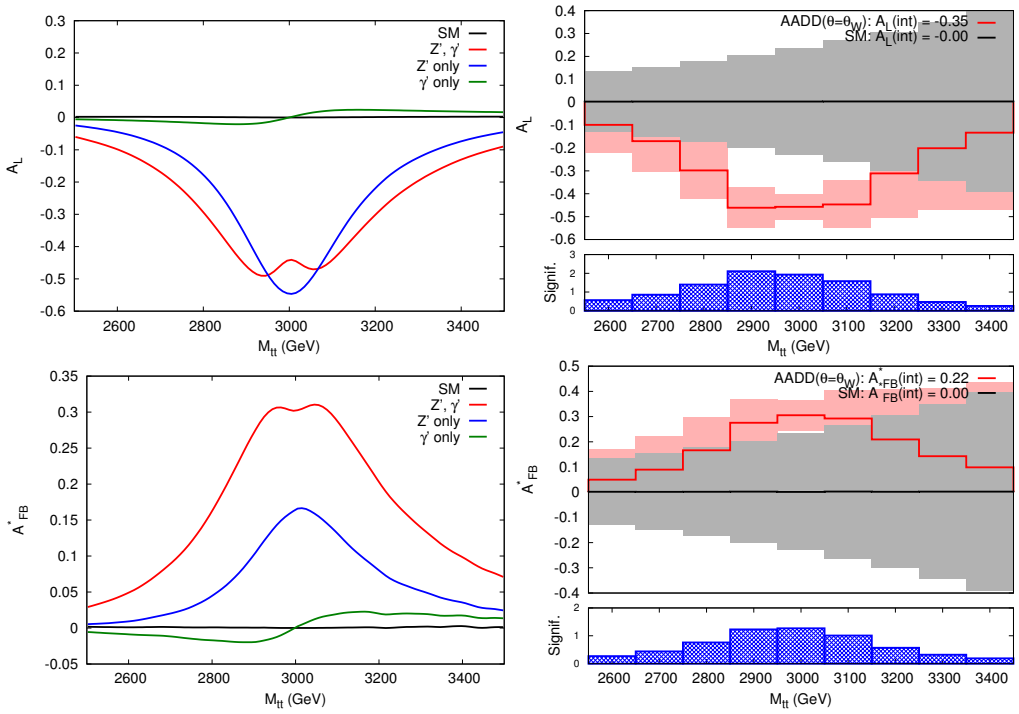

Figure 4: Identical plots to Figure 3 except where the couplings are Z-like and γ-like ($\theta = \theta_W$) instead. This corresponds to the unphysical case where off-diagonal matrix elements have not been considered, resulting in differing phenomenology occuring with the variation of an unphysical parameter, θ.

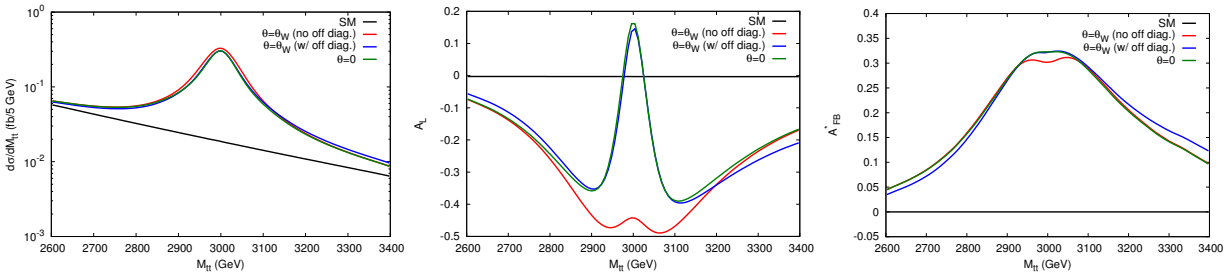

Figure 5: Differential distributions in $M_{t\bar{t}}$ for σ, A_L and A^*_{FB} comparing the mixed AADD with and without off diagonal width contributions to the unmixed case.

multiple resonances indicates that one may need to rely more on integrated quantities. In the next section we will show that the phenomenology of this model, displaying generic features of quasi-degenerate states, will allow it to be statistically separated from single resonance scenarios using only integrated asymmetries.

Before moving to the integrated analysis, we also present the previously shown observ-

ables in the split spectrum case ($M_{B'}$=2.98 TeV, $M_{W_3'}$=3.13 TeV), where the radiative mass corrections have been taken into account as described in Sect. 3.1. This drives the mass mixing to zero and brings the model to the edge of the quasi-degenerate regime. Namely, the splitting – of order 150 GeV – becomes comparable to the estimated mass resolution and corresponds to about 5% of R^{-1}. We see in Figure 6 that both the invariant mass distribution and the forward-backward asymmetry still do not resolve two distinct peaks. The spin polarisation asymmetry, A_L, however, clearly distinguishes between the opposing contributions of the two peaks in an even more striking way than in the degenerate case because the two contributions no longer have to compete at the same invariant mass. Another consequence of this is that the integrated value becomes closer to zero. As we will show in the next section, a single resonance does not generate a forward-backward asymmetry without simultaneously generating a polarisation asymmetry. Thus, the cancellation in the integrated prediction of A_L combined with a nonzero A^*_{FB} will serve as our distinguishing feature.

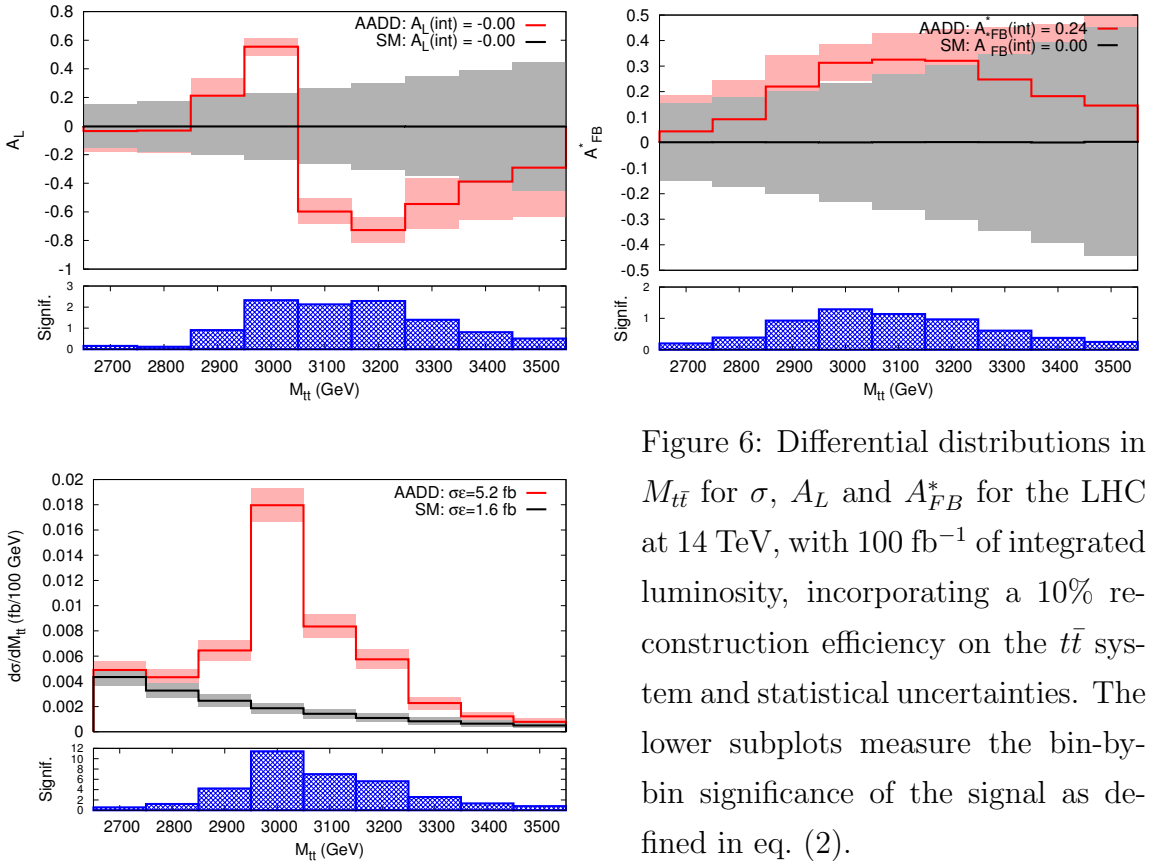

Figure 6: Differential distributions in $M_{t\bar{t}}$ for σ, A_L and A^*_{FB} for the LHC at 14 TeV, with 100 fb^{-1} of integrated luminosity, incorporating a 10% reconstruction efficiency on the $t\bar{t}$ system and statistical uncertainties. The lower subplots measure the bin-by-bin significance of the signal as defined in eq. (2).

4.2 Degeneracy versus a single resonance

Having confirmed that the presence of multiple degenerate resonances alters the phenomenology of asymmetry observables, we can explicitly use this to distinguish AADD from models with a single resonance. In order to provide a testbed for this, we created a set of 'toy' models of a single resonance designed to be indistinguishable from the degenerate AADD model in a resonance search. This was done by tuning the widths and the couplings and establishing appropriate parameters such that the invariant mass distribution of the points matched those of the AADD. This is shown in Figure 7, which represents a random selection of 3 points fulfilling these conditions. The minimal assumption of universal couplings across fermion generations was made in order to simplify the parameter scan, leaving only the up and down-type chiral couplings $u_{L,R}$ and $d_{L,R}$ as inputs. The other frequent assumption associated with Z's of fixing the charges of each SM representation was ignored, as requiring $u_L = d_L$ was over-constraining for a toy model, not necessarily meant to represent a physically motivated scenario coming from any particular gauge group extension. The distributions confirm that there are many possible combinations for values of charge and spin asymmetries for seemingly identical resonance cross sections. This is, of course, not surprising following our discussion of the couplings dependences of the various observables in Sect. 2.4 which also implies that the two asymmetry observables are correlated due to their identical dependence on the final state couplings. Again, we note that the observables in AADD remain distinguishable from any of the lettered benchmarks.

With this in mind, we performed a scan over all possible up and down-type couplings allowed while keeping the single resonance cross section (65 fb integrated 500 GeV either side of the resonance) and line-shape (i.e., width) fixed in order to compare and cross-correlate the two asymmetry observables. In addition, we also performed a less constrained parameter scan over any combination of couplings and a random choice of width to see whether the separation power of the asymmetries still holds. The couplings were sampled over an interval $\{0, 1\}$ while the widths were chosen to be a random value $\leq 10\%$ of the mass (3 TeV). Both sets of points are shown in Figure 8, where the AADD case is plotted as an ellipse representing the 1σ statistical uncertainties in the asymmetries. The tree-level SM prediction is included for reference, matching the case when the up-type couplings of a single resonance are purely vector-like ($u_L = u_R$). The observables plotted are integrated values of the asymmetry over an invariant mass of 500 GeV, for the LHC at 14 TeV and 100 fb^{-1} of integrated luminosity, with statistical uncertainty and reconstruction efficiency estimates consistent with the rest

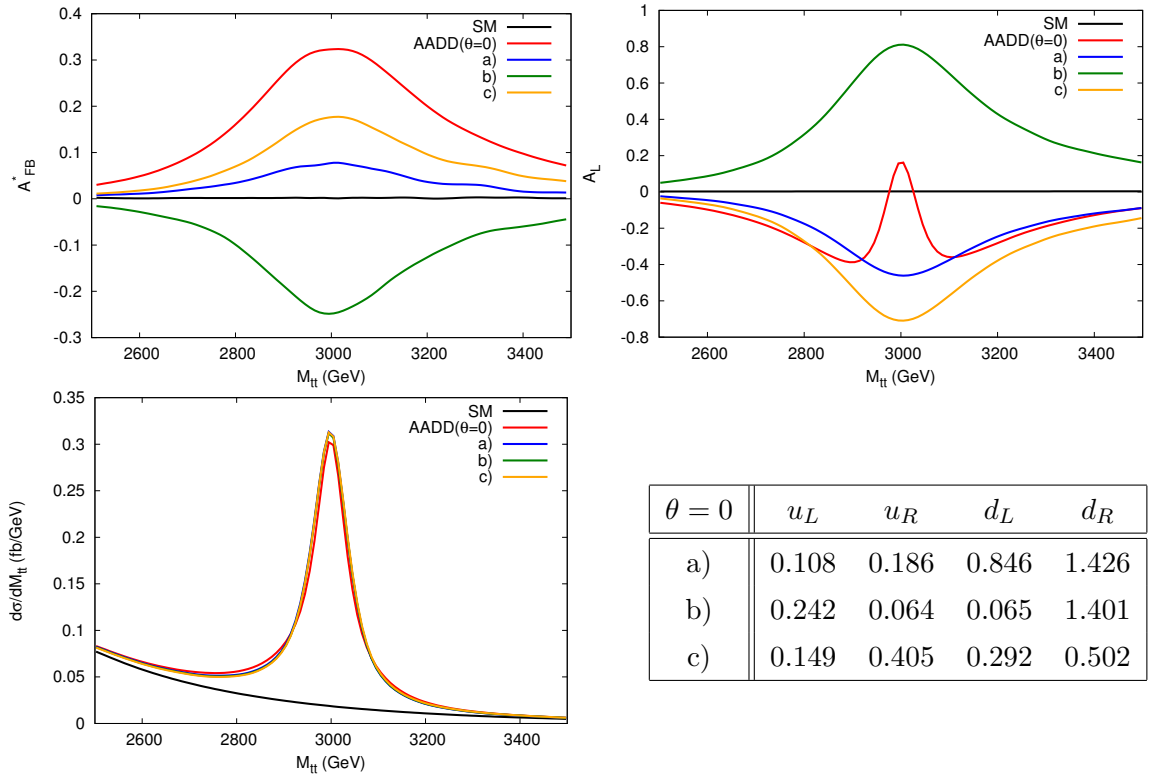

$\theta = 0$	u_L	u_R	d_L	d_R
a)	0.108	0.186	0.846	1.426
b)	0.242	0.064	0.065	1.401
c)	0.149	0.405	0.292	0.502

Figure 7: Differential distributions in $M_{t\bar{t}}$ for σ, A_L and A^*_{FB} comparing the AADD with three selected scan points modelling a single resonance with random couplings generated with its withs fixed to match the cross section of each case of AADD. The randomoly chosen couplings are summarised in the lower right table.

of this study.

Firstly, we confirm that the AADD scenario is distinguishable from the SM background in either observable. The profiles of the single resonance scan points show a clear quadratic relationship between the two observables. This can be understood if one assumes that the up quark initial state dominates the production: A_L will be proportional to the parity asymmetric coupling combination while A^*_{FB} will go as the square of this quantity as discussed in Sect. 2.4. In the case where the invariant mass distribution was constrained to match the AADD rate, the maximum values of A_L and A^*_{FB} are bounded by the maximum absolute value of the couplings. In the unconstrained scan, with the area covered by the points widens slightly due to the larger possible S/B, A_L becoming unbounded while A_{FB} is limited to be positive and somewhat less than A_L. This can, again, follows from the coupling dependence of both observables. The parameter scans show that the AADD resonances, in

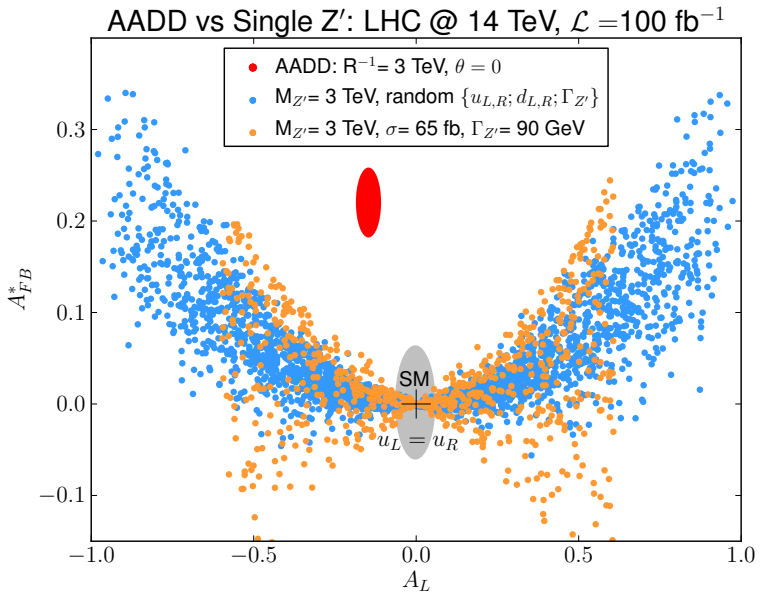

Figure 8: Scatter plots showing predicted values of A_L and A^*_{FB} for AADD with $R^{-1} = 3$ TeV at the LHC, compared to two sets of points. The first represents a scan over random couplings of a single 3 TeV resonance with a fixed width constrained to match the AADD invariant mass distribution (Figure 7). The second shows a scan where the couplings are randomly chosen over the ranges $\{0, 1\}$ and the resonance width is randomly chosen to be $\leq 10\%$ of the mass. The tree-level SM value is shown for reference and ellipses represent the 1σ statistical uncertainties as defined in Sect. 2.

the degenerate limit, can be fully disentangled from any possible single resonance that may produce a similar invariant mass profile in a bump-hunt, within our simplified treatment of reconstruction efficiencies and uncertainties. Therefore this suggests that in the scenario that multiple resonances are observed at the LHC but are masked by a quasi-degeneracy, one may be able to use the asymmetry observables to tell that the signal is coming from more than one resonance. Indeed, any signal appearing as a single peak, with asymmetry values outside of the area spanned by the points in Figure 8 will be a smoking gun for degenerate multiple-resonance physics.

5 Conclusions

We have established a realistic example of a model (denoted as AADD) of two quasi-degenerate resonances preferentially decaying to $t\bar{t}$ final states. Furthermore, the presence

of the two new particles cannot be distinguished from a generic single resonance scenario in bump-hunt searches. We have explained that the radiative mass corrections are important and induce splittings that bring the model towards the edge of the quasi-degenerate scenario. However, we have calculated them to be about 5% of the compactification scale, R^{-1}, and maintain that the splittings remain below the $t\bar{t}$ and dijet mass resolutions. In our discussion of radiative mass splittings, quasi degeneracy and subsequent mass mixing, we underlined the importance of a correct treatment of off-diagonal width contributions in this regime. By first considering the degenerate limit as a 'worst case scenario' for our purposes, we found that the omission of off diagonal-widths led to potentially misleading artifacts which made the mass mixing angle, θ, appear as a physical parameter even though it should not have. We used the latest LHC results from dijet and $t\bar{t}$ resonance searches to instruct ourselves on rough limits on the compactification scale from resonance searches at the LHC in order to examine a viable model.

Having expanded on the properties of asymmetry observables in terms of the couplings of said new resonances, we have demonstrated that both charge and spin asymmetries are required to distinguish our scenario from not only any singly resonant signal which mimics the invariant mass distribution of the our model but also any possible observed narrow resonance in $t\bar{t}$ searches. This is owed to the unique features of said asymmetries, that cannot be reproduced in the presence of only one resonant state decaying to $t\bar{t}$ pairs. In fact, this analysis can serve to probe similar models of multiple quasi-degenerate resonances and a prediction for A_L, A_{FB}^* from such a model lying outside the possible values for a single resonance is likely and would signal the presence of multiply resonant physics.

All our results have been obtained at parton level, yet in presence of realistic statistical uncertanties and reconstruction efficiencies, so they should undergo a certain degree of scrutiny in presence of $t\bar{t}$ decays, parton shower and hadronisation. However, we expect that the main conclusions of our work will not change substantially. In addition, the likely boosted nature of the top final state may suggest the need for alternative techniques for measuring top polarisation which do not rely on reconstructing the invariant mass of the top pair. It remains to be seen how the upgraded LHC will be able to deal with spin measurments in boosted tops, but what is clear is that, should they manage to measure the quantity with sufficient accuracy, it would shed much light on the coupling structure and potentially degenerate nature of an observed Z'.

Acknowledgments

We would like to thank Ignatios Antoniadis, Matthew Brown and Giacomo Cacciapaglia for significant help in understanding the many facets of the model studied here. SM is supported in part through the NExT Institute. KM is funded by STFC.

References

[1] I. Antoniadis, *Phys. Lett.* **B246** (1990) 377.

[2] N. Arkani-Hamed, S. Dimopoulos and G. Dvali, *Phys. Lett.* **B429** (9198) 263; I. Antoniadis, N. Arkani-Hamed, S. Dimopoulos and G. Dvali, *Phys. Lett.* **B436** (1998) 257.

[3] I. Antoniadis and C. Bachas, *Phys. Lett.* **B450** (1999) 83.

[4] J.D. Lykken, *Phys. Rev.* **D54** (1996) 3693; I. Antoniadis and B. Pioline, *Nucl. Phys.* **B550** (1999) 41; K. Benakli and Y. Oz, hep-th/9910090.

[5] K. Benakli, *Phys. Rev.* **D60** (1999) 104002; C.P. Burgess, L.E. Ibáñez and F. Quevedo, *Phys. Lett.* **B447** (1999) 257.

[6] G. Shiu and S.-H.H. Tye, *Phys. Rev.* **D58** (1998) 106007; Z. Kakushadze and S.-H.H. Tye, *Nucl. Phys.* **B548** (1999) 180; L.E. Ibáñez, C. Muñoz and S. Rigolin, hep-ph/9812397; G. Aldazabal, L.E. Ibáñez and F. Quevedo, hep-th/9909172.

[7] I. Antoniadis and K. Benakli, *Phys. Lett.* **B326** (1994) 69.

[8] I. Antoniadis, C. Muñoz and M. Quirós, *Nucl. Phys.* **B397** (1993) 515; I. Antoniadis, K. Benakli and M. Quirós, *Phys. Lett.* **B331** (1994) 313; K. Benakli, *Phys. Lett.* **B386** (1996) 106; I. Antoniadis and M. Quirós, *Phys. Lett.* **B392** (1997) 61; I. Antoniadis, S. Dimopoulos and G. Dvali, *Nucl. Phys.* **B516** (1998) 70; A. Pomarol and M. Quirós, *Phys. Lett.* **B438** (1998) 225; I. Antoniadis, S. Dimopoulos, A. Pomarol and M. Quirós, *Nucl. Phys.* **B544** (1999) 503; A. Delgado, A. Pomarol and M. Quirós, hep-ph/9812489.

[9] P. Nath and M. Yamaguchi, hep-ph/9902323 and hep-ph/9903298; M. Masip and A. Pomarol, hep-ph/9902467; W.J. Marciano, *Phys. Rev.* **D60** (1999) 093006; A. Stru-

mia, hep-ph/9906266; R. Casalbuoni, S. De Curtis, D. Dominici and R. Gatto, hep-ph/9907355; C.D. Carone, hep-ph/9907362.

[10] A. Delgado, A. Pomarol and M. Quirós, hep-ph/9911252.

[11] I. Antoniadis, K. Benakli and M. Quiros, *Phys. Lett.* **B460** (99) 176.

[12] P. Nath, Y. Yamada and M. Yamaguchi, hep-ph/9905415; T.G. Rizzo and J.D. Wells, hep-ph/9906234; T.G. Rizzo, hep-ph/9909232.

[13] L. Basso, K. Mimasu and S. Moretti, *JHEP* **1209** (2012) 024, *JHEP* **1211** (2012) 060, arXiv:1209.3622 [hep-ph], arXiv:1211.5470 [hep-ph] and arXiv:1211.5599 [hep-ph]; D. Barducci, S. De Curtis, K. Mimasu and S. Moretti, arXiv:1212.5948 [hep-ph].

[14] D. Krohn, T. Liu, J. Shelton and L. -T. Wang, Phys. Rev. **D84** (2011) 074034.

[15] R. W. Brown, D. Sahdev and K. O. Mikaelian, *Phys. Rev. Lett.* **43** (1979) 1069; J. H. Kuhn and G. Rodrigo, *Phys. Rev.* **D59** (1999) 054017.

[16] S. Moretti, M. R. Nolten and D. A. Ross, *Phys. Lett.* **B639** (2006) 513 [Erratum, *ibidem* **B660** (2008) 607]; S. Moretti and D. A. Ross, *Phys. Lett.* **B712** (2012) 245; J. H. Kuhn, A. Scharf and P. Uwer, *Eur. Phys. J.* **C45** (2006) 139 and *ibidem* **51** (2007) 37; W. Hollik and M. Kollar, *Phys. Rev.* **D77** (2008) 014008 and arXiv:0710.2472 [hep-ph]; W. Bernreuther, M. Fucker and Z. G. Si, Int. J. Mod .Phys. **A21** (2006) 914, *Phys. Rev.* **D78** (2008) 017503 and Nuovo Cim. **123** B (2008) 1036.

[17] T. Stelzer and S. Willenbrock, *Phys. Lett.* **B374** (1996) 169; G. Mahlon and S.J. Parke, *Phys. Rev.* **D53** (1996) 4886 and *ibidem* **81** (2010) 074024; W. Bernreuther, A. Brandenburg, Z.G. Si and P. Uwer, *Phys. Rev. Lett.* **87** (2001) 242002 and hep-ph/0410197; R. M. Godbole, K. Rao, S. D. Rindani and R. K. Singh, *JHEP* **1011** (2010) 144.

[18] S. Chatrchyan *et al.* [CMS Collaboration], CMS-PAS-JME-10-013; G. Aad *et al.* [ATLAS Collaboration], ATLAS-CONF-2012-065.

[19] G. Aad *et al.* [ATLAS Collaboration], JHEP **1301** (2013) 116 and JHEP **1209** (2012) 041; S. Chatrchyan *et al.* [CMS Collaboration], JHEP **1209** (2012) 029.

[20] J. Shelton, Phys. Rev. D **79** (2009) 014032; D. Krohn, J. Shelton and L. -T. Wang, JHEP **1007** (2010) 041.

[21] T. Appelquist, H. -C. Cheng and B. A. Dobrescu, *Phys. Rev.* **D64** (2001) 035002.

[22] E. Accomando, I. Antoniadis and K. Benakli, *Nucl. Phys.* **B579** (2000) 3.

[23] H. -C. Cheng, K. T. Matchev and M. Schmaltz, *Phys. Rev.* **D66** (2002) 036005.

[24] G. Cacciapaglia, A. Deandrea and S. De Curtis, *Phys. Lett.* **B682** (2009) 43.

[25] S. Chatrchyan *et al.* [CMS Collaboration], CMS-PAS-EXO-12-016,CMS-PAS-EXO-12-059.

[26] S. Chatrchyan *et al.* [CMS Collaboration], CMS-PAS-EXO-11-093.

[27] C. T. Hill, *Phys. Lett.* **B266** (1991) 419 and *Phys. Lett.* **B345** (1995) 483.

[28] H. Murayama, I. Watanabe and K. Hagiwara, KEK Report 91–11, January 1992.

[29] T. Stelzer and W. F. Long, *Comput. Phys. Commun.* **81** (1994) 357.

[30] J. Pumplin, D. R. Stump, J. Huston, H. L. Lai, P. Nadolsky and W. K. Tung, *JHEP* **07** (2002) 012.

[31] G. P. Lepage, *J. Comp. Phys.* **27** (1978) 192 [Erratum, preprint CLNS-80/447, March 1980].